nature communications

Article

https://doi.org/10.1038/s41467-026-71745-w

Primary cilia in the hypothalamic AgRP neurons mediate metabolic effects of butyrate

Received: 22 May 2025

Accepted: 31 March 2026

Published online: 09 April 2026

Check for updates

Santosh Rijal[1,4], Dong Joo Yang[1,4], Khanh Van Doan[1,2,4], Sang Hee Lyoo[1,3,4], Aran Lee[1,3], Yun-Hee Choi[1], Dong Min Shin[1] & Ki Woo Kim[1,3]

The microbiota-derived short-chain fatty acid (SCFA), butyrate influences host metabolism beyond the gut, including central regulation of appetite and energy homeostasis. However, mechanistic insights into central butyrate metabolic actions are undetermined. Here, we demonstrated that primary cilia of agouti-related peptide (AgRP) neurons in the hypothalamic arcuate nucleus are essential for butyrate's anorexigenic effects and glucose homeostasis. Notably, peripheral or central butyrate administration to the mice significantly enhanced hypothalamic ciliogenesis, possibly through increased histone acetylation and activation of ciliogenic transcription factors, leading to suppressed food intake and improved metabolism. Disrupting cilia in the hypothalamus or specifically in AgRP neurons, but not in ventromedial hypothalamus neurons, abolished these effects. At the neuronal level, butyrate inhibited AgRP neuron activity, and this effect was markedly reduced following primary cilia deletion, indicating that cilia are crucial for butyrate's inhibitory action. These findings establish primary cilia in AgRP neurons as essential mediators of butyrate's metabolic effects.

Microbiota-derived short-chain fatty acids (SCFAs), produced through the bacterial fermentation of indigestible dietary fiber, are suggested to play an essential role in gut-brain communication[1,2]. In addition to their local effects in the colon, increasing evidence supports that SCFAs, particularly butyrate, circulate beyond the gut to act on other organs, including the central nervous system (CNS), thereby affecting systemic homeostasis[3–10]. At physiological levels, butyrate is proposed to modulate brain functions indirectly through immune, endocrine, and vagal pathways[1]. However, at the higher concentrations used in most in vivo studies, butyrate may cross the blood-brain barrier (BBB), accumulate in the brain, and directly affect CNS functions[11–13]. Furthermore, SCFAs have been shown to regulate energy metabolism, potentially through central homeostatic mechanisms[3,4,7,8,10,14]. However, direct evidence that butyrate acts directly on central neurons (CNs) to regulate whole-body metabolism is lacking, and the molecular mechanisms underlying these CNS-mediated effects of butyrate remain to be elucidated.

Butyrate can influence host metabolism either as a cellular energy substrate or by altering host cellular functions and epigenetics. It acts on its receptors, such as G-protein coupled receptors (GPCRs) GPR109A and GPR41/43, or by inhibiting histone deacetylase (HDAC) enzymes[2,15–17]. HDACs are important factors in neural development and are associated with many brain disorders[18]. Butyrate's inhibition of HDACs has been implicated in its beneficial effects across a wide range of neurological diseases[19]. Recent studies suggest that HDACs are involved in the dysfunction of primary cilia, small organelles that act as cellular hubs regulating diverse signaling pathways under various health and disease conditions[20–27]. Furthermore, many cellular signaling pathways evoked by primary cilia involve different GPCRs, and primary cilia function is required for the localization and trafficking of

[1]Division of Physiology, Department of Oral Biology, Yonsei University College of Dentistry, Seoul 03722, Korea. [2]School of Health Sciences, Eastern International University, Binh Duong, Ho Chi Minh city 75121, Vietnam. [3]Department of Applied Life Science, BK21 FOUR, Yonsei University College of Dentistry, Seoul 03722, Korea. [4]These authors contributed equally: Santosh Rijal, Dong Joo Yang, Khanh Van Doan, Sang Hee Lyoo. e-mail: kiwoo-kim@yuhs.ac

metabolic receptors, including GPCRs, at the ciliary membrane[28–32]. Hypothalamic primary cilia have recently been demonstrated to play a critical role in the regulation of whole-body energy homeostasis[29,32–39]. This body of evidence raises the intriguing question of whether the SCFA butyrate directly modulates hypothalamic primary cilia function to promote its metabolic actions.

In the current study, we examined this hypothesis and demonstrated that primary cilia in hypothalamic AgRP neurons mediate the effects of butyrate on appetite and glucose homeostasis. We found that butyrate treatment, whether administered peripherally or centrally, significantly promoted hypothalamic ciliogenesis and improved whole-body glucose homeostasis, primarily through the suppression of energy intake. These metabolic effects of butyrate were abolished by disrupting primary cilia throughout the hypothalamus or specifically in AgRP neurons, but not by disrupting cilia in ventromedial hypothalamic (VMH) neurons. At the cellular level, we observed that the deletion of primary cilia specifically in AgRP neurons attenuated butyrate's inhibitory effect on these neurons. Collectively, these findings indicate that the SCFA butyrate directly targets primary cilia in hypothalamic AgRP neurons to exert its anorexigenic effect and confer metabolic benefits.

Results

Central butyrate regulates food intake and glucose homeostasis

To determine whether central administration of butyrate is sufficient to elicit systemic metabolic effects, 2.5 μL of butyrate (1.25 μg/μL) was administered into the hypothalamic third ventricle (3 V) of mice via intracerebroventricular (ICV) injection. The dose was selected to enhance histone acetylation without causing adverse neurological effects, such as seizures, sluggishness, or impaired feeding behavior[40,41]. In male mice maintained on a normal chow diet, 3 weeks of ICV administration of butyrate led to a significant reduction in body weight, accompanied by decreased food intake (Fig. S1a–d). Prolonged ICV butyrate treatment also protected male mice from high-fat diet (HFD)-induced weight gain and adipose hypertrophy in major fat depots, including epididymal (eWAT) and subcutaneous white adipose tissues (scWAT) (Fig. 1a–e). In female mice fed normal chow, ICV butyrate administration was limited to 1 week, rather than 3 weeks as in males, because their lower body weight (~24 g) made them more vulnerable to repeated long-term injections that could compromise their health. Under this short-term regimen, only a trend toward decreased body weight was observed, suggesting that 1 week of butyrate treatment is insufficient to induce significant body weight reduction in females (Fig. S1e–g). After 3 weeks of treatment, HFD-fed male mice receiving butyrate showed improved glucose tolerance and insulin sensitivity, although basal glucose and insulin levels remained unchanged (Fig. 1f–i).

To further explore the metabolic effects of central butyrate, we conducted indirect calorimetry to assess its impact on energy homeostasis. Mice receiving butyrate displayed a significant reduction in daily food intake without any notable changes in energy expenditure or locomotor activity (Fig. 1j–n). Concomitant with the significant reduction in food intake, butyrate treatment resulted in the downregulation of hypothalamic neuropeptide Y (*Npy*) and *Agrp* gene expresssion, both of which are crucial orexigenic neuropeptides (Fig. 1o). In addition, central butyrate administration was linked to reduced plasma leptin levels and a targeted enhancement of hypothalamic Signal transducer and activator of transcription 3 (STAT3) activation, collectively suggesting an increase in leptin sensitivity (Fig. 1p, q).

Butyrate directly modulates hypothalamic primary cilia

To seek direct evidence of butyrate actions in the hypothalamus, we examined the expression of its cellular targets in the hypothalamus both in vivo and in vitro. We found that several histone deacetylases (HDACs), including Class I and IIa, are expressed in both the mouse hypothalamus and hypothalamic N38 cells (Fig. S2a). We further examined whether butyrate could also directly induce neuronal HDAC inhibition by assessing histone acetylation under butyrate treatment. We observed that butyrate treatment significantly increased acetylation at several lysine residues on histones 3 (H3) and 4 (H4) in a dose- and time-dependent manner (Figs. 2a and S2b). This effect of butyrate on HDAC inhibition was evident at concentrations as low as 10 μM and became more prominent at concentrations equal to or higher than 1 mM (Fig. 2a). Notably, this HDAC inhibitory effect was specific to butyrate, as the ketone body β-hydroxybutyrate (BHB) did not alter histone acetylation even at high doses (Fig. S2c).

HDAC inhibition is associated with cilia expression, and hypothalamic cilia are known to be critical organelles for whole-body energy homeostasis[21–25,38,39,42]. Therefore, we next investigated whether butyrate is connected to primary cilia function in hypothalamic neurons. We first treated cells with 1 mM butyrate for 24 h and examined the expression of several transcriptional regulators involved in ciliogenesis. As shown in Fig. 2b, butyrate treatment significantly induced the expression of regulatory factor X (*Rfx*) isoforms 2 and 3, both known as cilia-promoting transcription factors[43,44]. Additionally, it markedly enhanced the transcription of various ciliary component genes involved in intraflagellar transport and the kinesin superfamily, resulting in a significant increase in both the number and length of primary cilia in hypothalamic N38 cells (Fig. 2c, d). Furthermore, direct ICV injection of butyrate into the third ventricle significantly enhanced histone acetylation and induced the expression of *Foxj1, Rfx2*, and *Rfx3*, and was notably associated with elongated primary cilia in several hypothalamic nuclei, including the arcuate nucleus (ARC) and the VMH (Fig. 2e–g).

Given that butyrate crosses the blood-brain barrier and potentially influences epigenetic processes in the brain[45], we investigated whether the metabolic benefits of peripheral butyrate administration are mediated through HDAC inhibition and associated alterations in primary cilia function within the hypothalamus. To test this, HFD-fed mice were treated with butyrate either orally or via intraperitoneal (i.p.) injection. For oral administration, sodium butyrate was supplied in the drinking water at a concentration of 100 mM, whereas mice in the i.p. group received daily injections of sodium butyrate at a dose of 500 mg/kg body weight. As shown in Fig. 2h–j (oral) and Fig. S2d–h (i.p.), butyrate treatment resulted in reduced body weight, decreased eWAT hypertrophy, and lower blood glucose levels. Notably, these metabolic improvements were accompanied by increased histone acetylation, along with a significant elongation of primary cilia in hypothalamic neurons (Figs. 2k, l and S2g, h). These findings suggest that butyrate may modulate histone acetylation and primary cilia function in the hypothalamus, contributing, at least in part, to its metabolic effects.

Hypothalamic primary cilia are essential for the metabolic effects of butyrate

We next investigated whether hypothalamic primary cilia are required for the metabolic actions of butyrate. To examine this, we stereotaxically injected recombinant adeno-associated virus serotype 2 (AAV2)—either encoding Cre recombinase fused to green fluorescent protein (AAV2-Cre-GFP) or lacking Cre (AAV2-GFP, control)—into the 3 V of the hypothalamus in mice carrying floxed alleles of intraflagellar transport protein 88 ($IFT88^{F/F}$) and a Cre-inducible tdTomato reporter at the ROSA26 locus ($ROSA26\text{-}tdTomato^{F/+}$) (Fig. 3a). Following vehicle or oral butyrate treatment (100 mM), we observed butyrate-induced primary ciliogenesis in AAV2-GFP–injected mice, whereas AAV2-Cre-GFP–injected mice showed specific deletion of primary cilia in the mediobasal hypothalamus, including the ARC and VMH (Figs. 3b and S3a, b). Different from the control virus-injected $IFT88^{F/F}$

https://doi.org/10.1038/s41467-026-71745-w

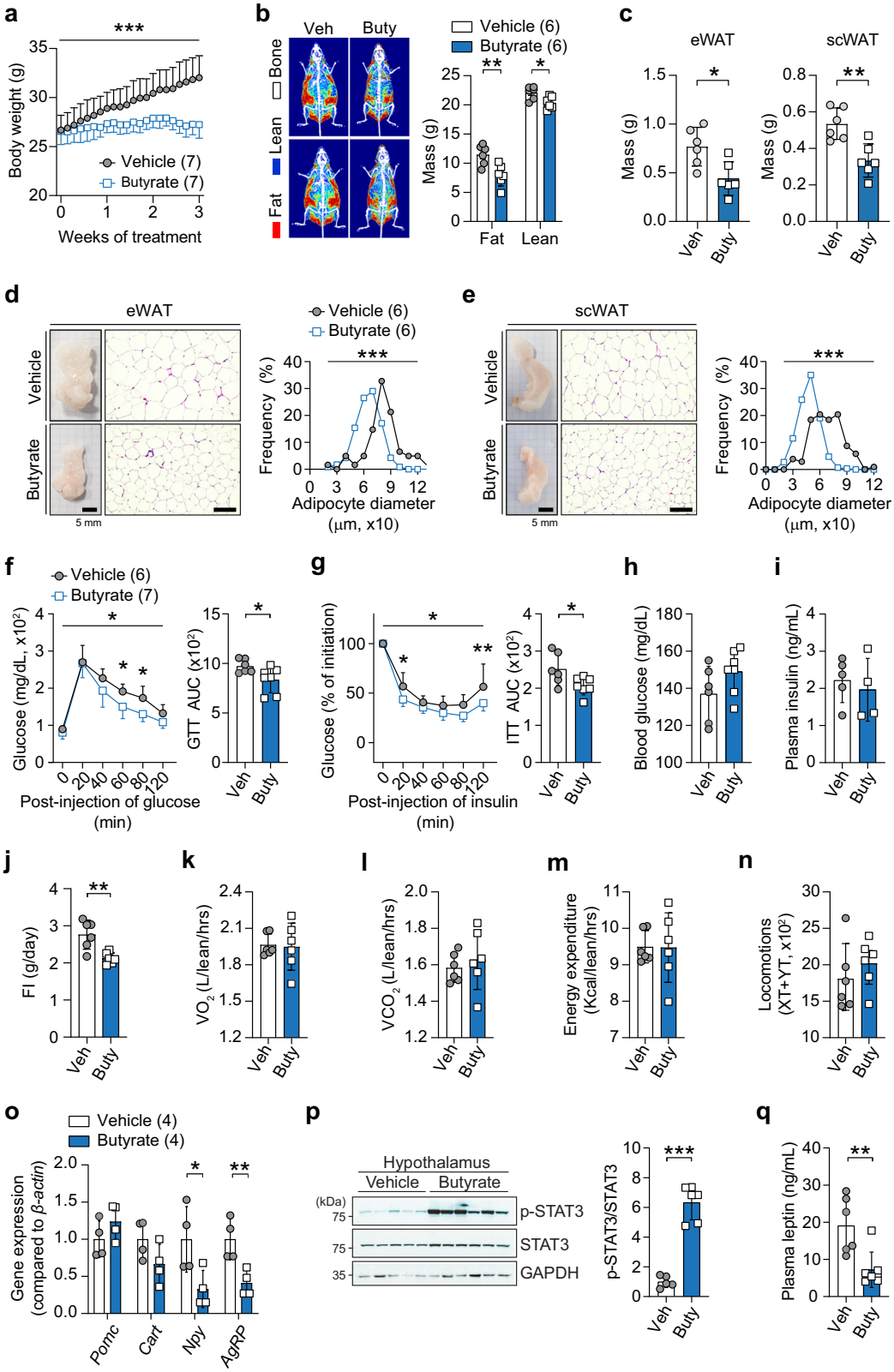

mice, the targeted deletion of primary cilia prevented hypothalamic ciliogenesis in response to butyrate (Fig. 3b).

Interestingly, the metabolic benefits of oral butyrate—such as reductions in body weight, fat mass, and food intake, as well as improvements in glucose and insulin homeostasis—observed in the control virus-injected group (Fig. 3c–h) were largely abolished in mice with disrupted primary cilia in the mediobasal hypothalamus (Fig. 3i–n). Notably, the beneficial effects on food intake and glucose tolerance were lost and became indistinguishable from those in control mice (Fig. 3e, g, k, m). Unexpectedly, butyrate-treated AAV2-Cre-GFP–injected mice exhibited increased body weight (Fig. 3c, d, i, j) and showed impaired insulin tolerance at a specific time point (Fig. 3h, n). These findings strongly suggest that hypothalamic primary cilia are crucial for mediating the metabolic

Fig. 1 | Direct central butyrate administration protects from diet-induced obesity and improves glucose homeostasis. a Body weight changes in HFD-fed mice injected ICV with butyrate or vehicle for 3 weeks ($n = 7$ mice per group). Two-way repeated-measures ANOVA followed by Sidak's multiple comparison test (***$p < 0.0001$). **b** Representative body composition images and comparison of fat and lean mass between groups after 3 weeks of ICV treatment. Two-tailed unpaired Student's *t*-test (fat mass, **$p = 0.0069$; lean mass, *$p = 0.0210$). **c** Mass of eWAT and scWAT isolated from HFD-fed mice treated with ICV butyrate or vehicle ($n = 6$ mice per group). Two-tailed unpaired Student's *t*-test (eWAT, *$p = 0.0118$; scWAT, **$p = 0.0030$). Representative H&E images and frequency distribution of adipocyte diameters in eWAT (**d**) and scWAT (**e**) of HFD-fed mice injected ICV with butyrate or vehicle ($n = 6$ mice for each group). Mann–Whitney *U* test (***$p < 0.0001$, respectively). Scale bars, 100 μm. **f** Glucose tolerance test (GTT) and area under the curve (AUC) in HFD-fed mice treated with ICV vehicle or butyrate for 3 weeks. Two-way repeated-measures ANOVA (*$p = 0.0397$) followed by Sidak's multiple comparison test for individual time points (60 min, *$p = 0.0361$; 80 min, *$p = 0.0278$). Two-tailed unpaired Student's *t*-test (AUC, *$p = 0.0405$). **g** Insulin tolerance test (ITT) and AUC in HFD-fed mice injected ICV with vehicle or butyrate (vehicle, $n = 6$; butyrate, $n = 7$). Two-way repeated measures ANOVA (*$p = 0.0313$) followed by Sidak's multiple comparison test for individual time points (20 min, *$p = 0.0499$; 120 min **$p = 0.0100$). Two-tailed unpaired Student's *t*-test (AUC, *$p = 0.0367$). Blood glucose ($n = 6$ for vehicle; $n = 7$ for butyrate) (**h**) and plasma insulin levels (vehicle, $n = 5$; butyrate, $n = 4$) (**i**) in HFD-fed mice after 3 weeks of ICV vehicle or butyrate administration. **j** Average daily food intake during 3rd week of ICV injection with butyrate or vehicle in HFD-fed mice ($n = 6$ mice per group). Two-tailed unpaired Student's *t*-test, (**$p = 0.0036$). Indirect calorimetry results in HFD-fed mice after 3 weeks of ICV butyrate or vehicle administration. Average VO_2 (**k**) and VCO_2 (**l**) energy expenditure (**m**) and locomotor activity (**n**) were measured in metabolic chambers ($n = 6$ mice per group). **o** Effects of central butyrate on the expression of appetite-regulating hypothalamic neuropeptides. Two-tailed unpaired Student's *t*-test (*Npy*, *$p = 0.0477$; *Agrp* **$p = 0.0010$). **p** Representative immunoblots and densitometric analysis showing the effects of central butyrate treatment on hypothalamic leptin signaling, assessed by p-STAT3 (vehicle, $n = 5$; butyrate, $n = 6$). Two-tailed unpaired Student's *t*-test (***$p < 0.0001$). **q** Plasma leptin levels in HFD-fed mice after 3 weeks of ICV vehicle or butyrate treatment (vehicle, $n = 6$; butyrate, $n = 7$). Two-tailed unpaired Student's *t*-test (**$p = 0.0055$). The number of mice used in each experiment is indicated in the corresponding panel. Data are presented as mean ± SD. The data for each figure are specified in associated Source data file.

effects of butyrate, particularly in the regulation of body weight and glucose homeostasis.

Primary cilia in the AgRP neuron of the ARC are required for the metabolic actions of butyrate

We next sought to identify the crucial neuronal populations in the hypothalamus whose primary cilia are responsible for mediating the metabolic effects of butyrate[35,37,38]. Among the hypothalamic regions, ARC and VMH are well-established centers involved in primary cilia-mediated regulation of energy metabolism[30,36–39]. Steroidogenic factor-1 (SF-1) neurons in the VMH are a well-characterized neuronal population that regulates energy balance through primary cilia[38]. In the ARC, the orexigenic peptides AgRP and NPY, which are key regulators of feeding behavior, were suppressed by butyrate treatment (Fig. 1o). Therefore, we generated two distinct knockout models to target SF-1 neurons in the VMH and AgRP neurons in the ARC, respectively. This was achieved by crossing $IFT88^{F/F}$ mice with either SF-1-cre (IFT88 $KO^{SF\text{-}1}$) or AgRP-cre (IFT88 KO^{AgRP}) mice (Fig. S4a). The SF-1 neuron- and AgRP neuron-specific IFT88 knockout mice exhibited no detectable cilia in these neurons, confirming the successful and targeted knockout (Fig. S4b, c).

In IFT88 $KO^{SF\text{-}1}$, central butyrate treatment significantly reduced body weight and food intake (Fig. 4a–c). The metabolic effects of central butyrate on leptin and insulin homeostasis (Fig. 4d, e) were also intact in IFT88 $KO^{SF\text{-}1}$ mice. Furthermore, butyrate improved glucose and insulin tolerance (Fig. 4f, g). However, these metabolic effects of butyrate were completely abolished in IFT88 KO^{AgRP} mice, highlighting that the primary cilia function in AgRP neurons is essential for the anorexigenic action of butyrate (Fig. 4h–n).

Butyrate inhibits AgRP neurons and requires primary cilia for its effect

Given that the metabolic effects of butyrate were abolished in IFT88 KO^{AgRP} mice, we next investigated whether primary cilia are required for butyrate's action on AgRP neurons using whole-cell patch clamp recordings (Fig. 5a). Primary cilia signaling has been reported to modulate neuronal excitability through receptors, ion channels, and secondary messengers, with electrophysiological evidence supporting both synaptic and intrinsic regulatory mechanisms[37,46]. To address this, we recorded the resting membrane potential (RMP) and spontaneous action potential (sAP) firing frequency in AgRP neurons from wild type (WT, AgRP-cre; $tdTomato^{F/+}$) and AgRP neuron-specific primary cilia knockout IFT88 KO^{AgRP} (AgRP-cre; $IFT88^{F/F}$; $tdTomato^{F/+}$) mice (Fig. 5b–d). Baseline measurements revealed no significant differences in either RMP or sAP firing frequency between the two groups (Supplementary Table 1).

To assess primary cilia's role in butyrate-induced regulation of AgRP neuron activity, we bath applied 1 mM butyrate for 3–4 min and observed variable response in both WT and IFT88 KO^{AgRP} neurons (Fig. 5e). The change in RMP following butyrate treatment was measured as the difference between the RMP before and after application. Upon butyrate application, 71% of tested WT neurons ($n = 15/21$) exhibited changes in RMP, predominantly hyperpolarization whereas 52% of tested IFT88 KO^{AgRP} neurons ($n = 12/23$) responded, showing either hyperpolarization (43%) or depolarization (9%) (Fig. 5f, h–i). The average hyperpolarization in WT neurons was −10.5 ± 2.13 mV ($n = 15$), while IFT88 KO^{AgRP} neurons showed a slightly reduced average hyperpolarization of −8.07 ± 1.55 mV ($n = 10$) (Fig. 5j). Depolarization observed only in IFT88 KO^{AgRP} neurons ($n = 2/23$) displayed average value of 5.07 ± 1.75 mV.

Additionally, butyrate also modulated sAP frequency. In most cases, the inhibition of sAP frequency was associated with hyperpolarization. However, in some instances, sAP frequency was altered without change in RMP, showing variable effects, including increase, decrease, or no change. Based on these observed effects on RMP and sAP activity, neurons were classified as inhibited, excited, or unaffected in both WT and IFT88 KO^{AgRP} groups. Butyrate application inhibited neuronal activity (via hyperpolarization and/or decreased sAP frequency) in the majority of WT neurons (81%) compared to IFT88 KO^{AgRP} neurons (48%). Conversely, a higher percentage of IFT88 KO^{AgRP} neurons (22%) were excited (via depolarization and/or increased sAP frequency) relative to WT neurons (14%) (Fig. 5g, k–l). However, no significant difference was observed between the two groups in the inhibition of sAP frequency by butyrate (Fig. 5m).

Primary cilia facilitate butyrate-mediated inhibitory signaling in AgRP neurons

Next, we investigated whether primary cilia in AgRP neurons contribute to synaptic activity by comparing spontaneous inhibitory post-synaptic currents (sIPSCs) and spontaneous excitatory post-synaptic currents (sEPSCs) between the two groups. Notably, IFT88 KO^{AgRP} neurons exhibited significantly reduced sIPSCs frequency and amplitude compared to WT neurons (Fig. 6a–c and Supplementary Table 1), whereas sEPSCs frequency or amplitude were unchanged (Fig. 6j–l and Supplementary Table 1). Based on these findings, we speculated that butyrate's effect on AgRP neuronal excitability may depend upon synaptic transmission. To test this, we examined butyrate's impact on sIPSCs and sEPSCs in WT and IFT88 KO^{AgRP} neurons. In WT AgRP

https://doi.org/10.1038/s41467-026-71745-w

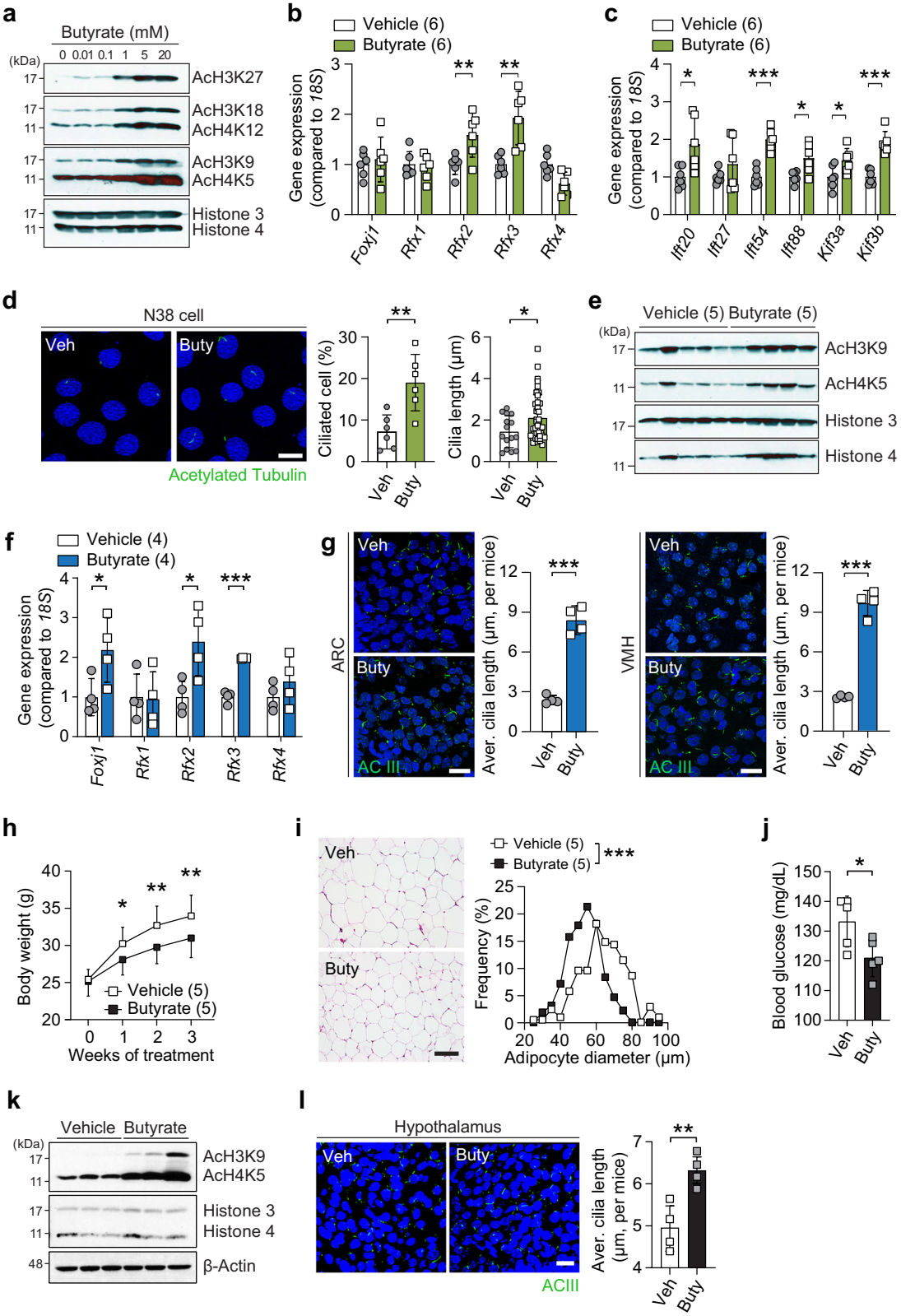

neurons, bath application of butyrate significantly increased sIPSCs frequency (Fig. 6d, e); however, this effect was not observed in IFT88 KO^{AgRP} neurons (Fig. 6g, h and Supplementary Table 2). Butyrate did not significantly alter sIPSCs amplitude in either group (Fig. 6f, i and Supplementary Table 2). Regarding sEPSCs, butyrate induced no significant changes in frequency or amplitude in either neuron type (Fig. 6m–r and Supplementary Table 2). Taken together, these results indicate that the inhibitory effect of butyrate on AgRP neurons is highly dependent on the presence of primary cilia and may underline its anorexigenic actions.

Discussion

A body of evidence has suggested that butyrate has various beneficial effects on metabolic and neurological conditions, and some of these

Fig. 2 | Butyrate promotes histone acetylation and primary cilia formation in the hypothalamus. a Butyrate-induced, dose-dependent changes in histone acetylation at specific lysine residues in hypothalamic N38 cells after 24 h treatment with butyrate. Effects of butyrate (1 mM, 24 h) on the expression of transcriptional regulators of ciliogenesis (**b**) and ciliary genes (**c**) in hypothalamic N38 cells ($n = 6$ technical replications). Two-tailed unpaired Student's *t*-test (*Rfx2*, $^{**}p = 0.0099$; *Rfx3*, $^{**}p = 0.0012$; *Ift20*, $^{*}p = 0.0196$; *Ift54*, $^{***}p < 0.0001$; *Ift88*, $^{*}p = 0.0174$; *Kif3a*, $^{*}p = 0.0412$; *Kif3b*, $^{***}p = 0.0001$). **d** Representative IF images and quantification graphs showing the effects of butyrate on the ratio of ciliated cells and ciliary length after 24 h incubation with butyrate (1 mM) ($n = 6$ technical replicates). Two-tailed unpaired Welch's *t*-test (% ciliated cells, $^{**}p = 0.0061$; cilia length, $^{*}p = 0.0184$). Scale bar, 20 μm. **e** Immunoblots showing the effects of central butyrate treatment on histone acetylation in the hypothalamus ($n = 5$ mice per group). **f** Effects of butyrate (1.25 μg/μL, 2.5 μL) on the expression of transcriptional regulators of ciliogenesis in the hypothalamus ($n = 4$ mice per group). Two-tailed unpaired Student's *t*-test (*Foxj1*, $^{*}p = 0.0440$; *Rfx2*, $^{*}p = 0.0251$; *Rfx3*, $^{***}p < 0.0001$). **g** Representative IF images and quantification showing ICV butyrate-induced changes in hypothalamic cilia length in the VMH and ARC ($n = 4$ mice per group). Two-tailed unpaired Student's *t*-test ($^{***}p < 0.0001$, respectively). Scale bar, 20 μm. **h** Body weight changes in HFD-fed mice following oral butyrate (100 mM) treatment ($n = 5$ mice per group). Two-way repeated-measures ANOVA followed by Sidak's multiple comparison test ($^{*}p = 0.0217$, $^{**}p = 0.0017$, and $^{**}p = 0.0015$). **i** H&E images and adipocyte size distribution in eWATs ($n = 5$ mice per group). Mann–Whitney U test ($^{***}p < 0.0001$). Scale bar, 100 μm. **j** Fed blood glucose levels after oral butyrate treatment ($n = 5$ mice per group). Two-tailed unpaired Student's *t*-test ($^{*}p = 0.0334$). **k** Effect of oral butyrate treatment on histone acetylation in the hypothalamus ($n = 3$ mice per group). **l** Representative immunostaining images and quantification showing the effect of oral butyrate on primary cilia length in the hypothalamus ($n = 4$ mice per group). Two-tailed unpaired Student's *t*-test ($^{**}p = 0.0070$). Scale bar, 20 μm. Cell culture experiments were performed in biological triplicates. Numbers in parentheses indicate the number of mice used. Values are presented as mean ± SD. The data for each figure are specified in associated Source data file.

effects are associated with histone deacetylase (HDAC) inhibition[1,19,47]. Recent studies have further demonstrated that HDACs are involved in the regulation of primary cilia, and that HDAC inhibition promotes the maintenance and elongation of primary cilia[20–25]. Consistent with these findings, our study suggests that butyrate-induced HDAC inhibition upregulates the ciliary transcription factors *Rfx2* and *Rfx3*, thereby promoting primary ciliogenesis in hypothalamic neurons. We further show that butyrate directly targets hypothalamic primary cilia to mediate its effects on feeding and glucose homeostasis. Notably, primary cilia in hypothalamic AgRP neurons are essential for the metabolic actions of butyrate on appetite and energy balance.

Short-chain fatty acids (SCFAs), including butyrate, have been shown to influence food intake and energy metabolism, potentially through central homeostatic mechanism in the hypothalamus[4,7,8,10]. Frost et al. demonstrated that systemically administered acetate crosses the blood-brain barrier, where it modulates hypothalamic AMPK activity and suppresses food intake and body weight gain by altering the expression of AgRP, NPY, and pro-opiomelanocortin (POMC) neuropeptides[14]. Consistently, Li et al. showed that the metabolic benefits of oral butyrate treatment were primarily mediated by its anorexigenic effect through the suppression of NPY neuron activity[4]. In line with these findings, our study showed that direct central butyrate administration improved whole-body glucose homeostasis and suppressed appetite and energy intake. These metabolic effects of butyrate were closely associated with a marked activation of the leptin/STAT3 pathway and a robust increase in primary ciliogenesis in the hypothalamus. Notably, hypothalamic ciliogenesis has been shown to be essential for an appropriate neuronal response to leptin-mediated satiety signaling[36]. A specific enhancement of the hypothalamic leptin-STAT3 signaling pathway, accompanied by increased hypothalamic ciliogenesis under central butyrate treatment, may account for its pronounced effects on appetite and body weight, given that hypothalamic STAT3 activation is essential for the anorexigenic action of leptin[48,49]. Importantly, disruption of primary cilia in the mediobasal hypothalamus, or specifically in AgRP neurons, abolished the metabolic effects of both peripheral and central butyrate administration, demonstrating that the SCFA butyrate exerts its systemic metabolic actions through direct effects on the hypothalamus. Interestingly, however, in mice with primary cilia ablated throughout the mediobasal hypothalamus, butyrate-treated animals exhibited greater body weight than vehicle-treated controls, despite no increase in food intake (Fig. 3i, k). We had initially expected that disruption of primary cilia in the mediobasal hypothalamus would simply abolish the anorexigenic and weight-lowering effects of butyrate, resulting in comparable body weight between vehicle- and butyrate-treated groups. Instead, the greater weight gain observed in butyrate-treated cilia-deficient mice suggests that loss of mediobasal hypothalamic cilia may alter energy balance in a more complex manner. One possibility is that deletion of primary cilia in this region impairs energy expenditure—such as thermogenesis or locomotor activity—thereby overriding the catabolic actions of butyrate. Another, not mutually exclusive, possibility is that the absence of primary cilia in the mediobasal hypothalamus engages energy-conserving or other counter-regulatory pathways, rather than merely blunting butyrate signaling, thereby predisposing cilia-deficient mice to greater weight gain than their vehicle-treated counterparts. We believe that future studies directly examining this phenotype, particularly in relation to energy expenditure, are warranted.

Butyrate incorporated into the diet at 5% wt/wt was used in most of rodent studies showing beneficial effects of oral butyrate administration against diet-induced obesity[4,8–10,50–52], which is comparable to a dose of 5 g/kg body weight, considering that a 30 g mouse consumes about 3 g of HFD every day[53]. This oral dose of butyrate was shown to produce peak plasma butyrate concentrations of approximately 10 mM, similar to a 500 mg/kg intravenous (i.v.) dose, and plasma butyrate levels remained higher than 1 mM for 90 min after dosing[54]. Plasma concentrations from these therapeutic doses of butyrate were much higher than its physiological levels produced from the gut microbiota[55]. Frost et al. using ^{11}C-acetate PET imaging in rats, demonstrated that approximately 3% of an i.v. acetate dose instantly enters the brain after injection, and more than 1% of the injected dose remains in the brain after 60 min of treatment[14]. Given that butyrate is the SCFA with the ability to cross the blood–brain barrier[12], we hypothesized that its accumulation in the central nervous system following chronic peripheral administration at therapeutic doses may be sufficient to inhibit HDACs and promote hypothalamic ciliogenesis. Indeed, peripheral administration of butyrate, either orally or intraperitoneally, led to significant increases in histone acetylation and primary ciliogenesis in the hypothalamus, similar to the effects observed with direct central administration into the 3 V.

The neuropharmacological effects of the SCFA butyrate have been largely considered indirect, mediated through immune, endocrine, or vagal pathways[1]. Li et al. proposed that the central effects of butyrate on food intake and energy metabolism are mediated indirectly via the vagal nerve. They observed that oral, but not i.v., administration of butyrate reduced chow intake, and this effect was abolished by total subdiaphragmatic vagotomy. Based on these findings, they suggested that butyrate acts through a vagal, rather than a direct central, mechanism[4]. However, in their study, butyrate was administered orally at relatively high doses (0.15 mL of a 6 M solution for acute treatment and 5% wt/wt in the HFD for chronic treatment), whereas the single i.v. dose tested (~60 mg/kg; 0.1 mL of a 150 mM solution per ~30 g mouse) was nearly tenfold lower than the i.v. dose required to replicate the plasma pharmacokinetics of a 5 g/kg oral

https://doi.org/10.1038/s41467-026-71745-w

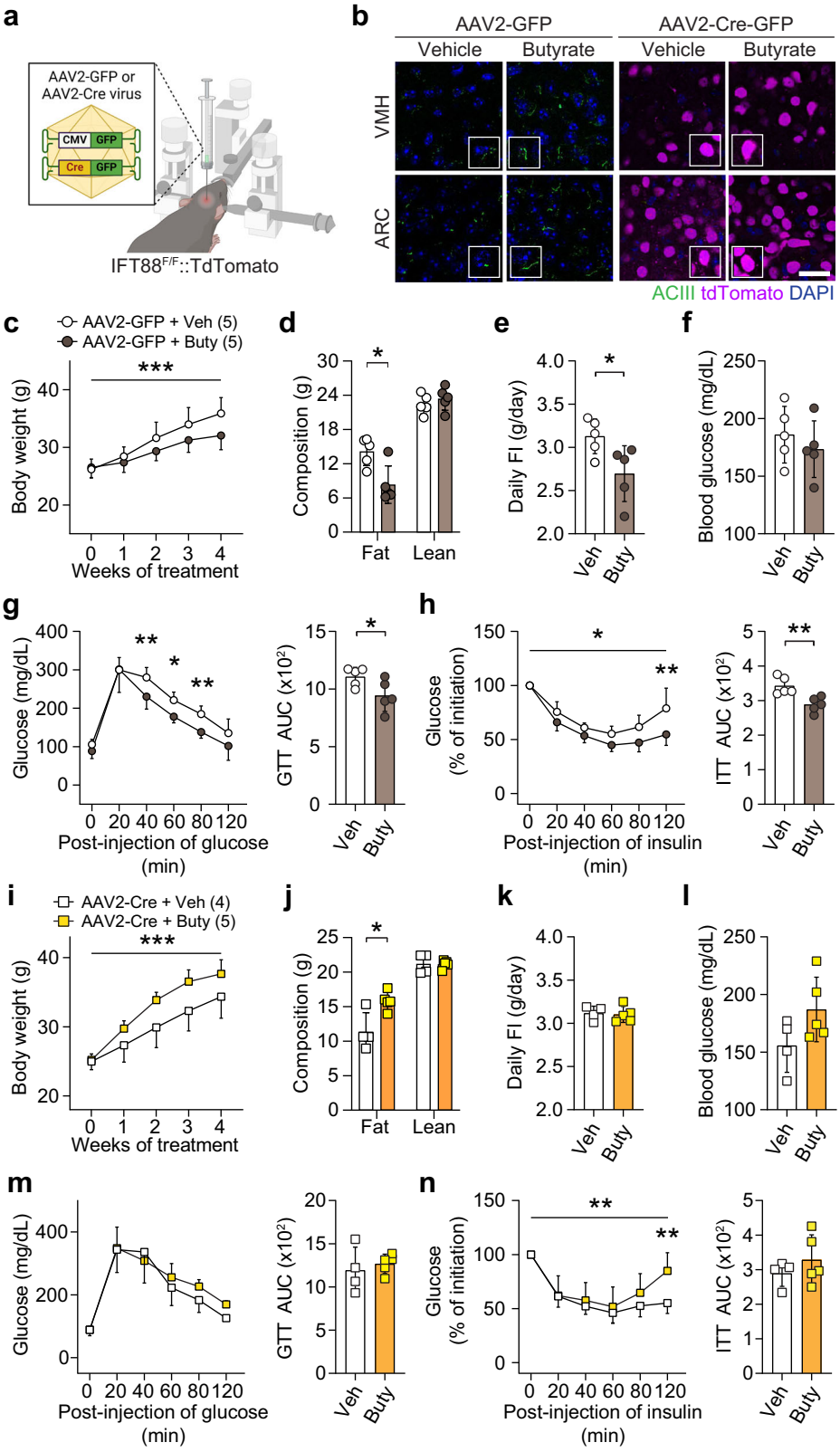

dose[54]. Moreover, the total subdiaphragmatic vagotomy performed in their study eliminated both afferent and efferent vagal fibers, disrupting bidirectional communication between the gut and the brain[4,56]. Therefore, although Li et al. emphasized the role of vagal afferents in mediating the metabolic effects of oral butyrate, the possibility of direct central actions cannot be ruled out. In this regard, our findings on butyrate-induced modulation of hypothalamic function provide direct evidence supporting a central mechanism mediating the metabolic actions of this SCFA.

One of the key findings of our study is the identification of AgRP neurons in the hypothalamus as the specific neuronal population whose primary cilia mediate the central metabolic actions of butyrate. Primary cilia in various hypothalamic neurons have been shown to play essential roles in regulating leptin signaling, body weight, and systemic

Fig. 3 | Disruption of primary cilia in the mediobasal hypothalamus abolishes the metabolic effects of butyrate. a Schematic illustration of AAV2-GFP (control) or AAV2-Cre-GFP injection into the mediobasal hypothalamus. The illustration image was created in BioRender. Kim, K. W. (2026) https://BioRender.com/zfjnc59. **b** Cre-driven tdTomato fluorescence confirms successful delivery of control AAV2-GFP or AAV2-Cre-GFP into the mediobasal hypothalamus. Primary cilia, visualized by ACIII staining, were absent in both the ARC and VMH of AAV2-Cre-GFP–infected mice. ACIII, adenylyl cyclase III. Scale bar, 20 μm. **c**–**f** Effects of oral butyrate treatment on body weight and compositions under HFD feeding. **c**, **d** Daily food intake (**e**), and blood glucose levels in the fed state (**f**) in IFT88$^{F/F}$ mice injected with AAV2-GFP control virus ($n = 5$ mice per each group). Two-way repeated-measures ANOVA followed by Sidak's multiple comparison test (weekly body weight, $^{***}p = 0.0002$). Two-tailed unpaired Student's *t*-test (fat mass, $^{*}p = 0.0134$; FI, $^{*}p = 0.0347$). **g** GTT and corresponding AUC in IFT88$^{F/F}$ mice injected with AAV2-GFP following 4 weeks of oral butyrate administration ($n = 5$ mice per group). Two-way repeated-measures ANOVA followed by Sidak's multiple comparison for individual time point (40 min, $^{**}p = 0.0028$; 60 min, $^{*}p = 0.0108$; 80 min $^{**}p = 0.0054$). Two-tailed unpaired Student's *t*-test (AUC, $^{*}p = 0.0499$). **h** ITT and corresponding AUC in IFT88$^{F/F}$ mice injected with AAV2-GFP ($n = 5$ mice per each group). Two-way repeated-measures ANOVA (significance in average values, $^{*}p = 0.0350$) with Sidak's multiple comparison test for individual time point (120 min, $^{**}p = 0.0016$). Two-tailed unpaired Student's *t*-test (AUC, $^{**}p = 0.0066$). Effects of oral butyrate treatment on body weight and compositions under HFD feeding (**i**, **j** daily food intake (**k**) and blood glucose levels in the fed state (**l**) in IFT88$^{F/F}$ mice injected with AAV2-Cre-GFP (vehicle, $n = 4$; butyrate, $n = 5$). Two-way repeated-measures ANOVA with Sidak's multiple comparison test (weekly body weight, $^{***}p < 0.0001$). Two-tailed unpaired Student's *t*-test (fat mass, $^{*}p = 0.0149$). **m** GTT and corresponding AUC in IFT88$^{F/F}$ mice injected with AAV2-Cre-GFP following 4 weeks of oral butyrate administration (vehicle, $n = 4$; butyrate, $n = 5$). **n** ITT (left) and corresponding AUC (right) in IFT88$^{F/F}$ mice injected with AAV2-Cre-GFP (vehicle, $n = 4$; butyrate, $n = 5$). Two-way repeated measures ANOVA ($^{**}p = 0.0037$) with Sidak's multiple comparison test for individual time points (120 min, $^{**}p = 0.0043$). The number of mice used is indicated in each figure panel in parentheses. Data are presented as mean ± SD. The data for each figure are specified in associated Source data file.

metabolic homeostasis[35–38]. For example, Guo et al. demonstrated that disruption of the ciliary component BBSome in either POMC or AgRP neurons, impaired the regulation of food intake and body weight[31,35]. Similarly, Lee et al. reported that deletion of ciliogenic genes such as IFT88 or KIF3B in POMC neurons disrupted developmental adiposity programming and long-term metabolic regulation[37]. Sun et al. also showed that deletion of IFT88 in VMH neurons compromised energy and skeletal homeostasis[38]. In our study, by systematically comparing the metabolic effects of butyrate across various hypothalamic cilia-deficient mouse models, we found that its anorexigenic and metabolic actions were abolished in mice with AgRP neuron-specific deletion of primary cilia (IFT88 KO^{AgRP}) and in mice with broad hypothalamic cilia disruption (AAV2-Cre; IFT88$^{F/F}$), whereas these effects were preserved in mice lacking primary cilia in SF-1 neurons (IFT88 KO^{SF-1}). These findings indicate that cilia-dependent signaling in AgRP neurons is required for butyrate's central metabolic effects. This interpretation is further supported by our electrophysiological data showing that butyrate directly inhibits AgRP neuronal activity, and that this inhibition is lost in the absence of functional primary cilia. Interestingly, our additional analysis revealed that primary cilia in AgRP neurons are significantly longer than those in POMC neurons, suggesting a structural basis that may underlie the heightened sensitivity of AgRP neurons to butyrate-induced ciliary signaling (Fig. S5). Collectively, our results establish that primary cilia in AgRP neurons are a critical cellular component mediating the anorexigenic actions of the SCFA butyrate.

Methods

Reagents and primary antibodies

Sodium butyrate and β-hydroxybutyrate (BHB) were purchased from Sigma-Aldrich (St. Louis, MO, USA) and dissolved in UltraPure™ water (Invitrogen, Waltham, MA, USA) in stock solutions. Stock solutions of butyrate and BHB were filtered through a 0.2 μm membrane and stored at −80 °C. Working solutions were freshly prepared by diluting the stock solutions with UltraPure™ water. Trichostatin A was purchased from Sigma and dissolved in DMSO. All chemicals were obtained from Sigma unless stated otherwise.

Antibodies against Histone 3 (Cat.no.4499), AcH3K9 (Cat.no.9649), AcH3K18 (Cat.no.13998), AcH3K27 (Cat.no.8173), STAT3 (Cat.no.9139), phosphorylated-STAT3 (Cat.no.9145), and a kit of HDACs antibodies (Cat.no.9928) were purchased from Cell Signaling Technologies (Danvers, MA, USA). Antibodies against Histone 4 (Cat.no.ab177840), AcH4K5 (Cat.no.ab519987), and AcH4K12 (Cat.no.ab177793) were obtained from Abcam (Cambridge, UK). Antibodies against Adenylyl cyclase III (Cat.no.sc-588) and GAPDH (Cat.no.sc-32233) were purchased from Santa Cruz Biotechnology (Dallas, TX, USA). Acetylated-α-tubulin (Cat.no.T7451) antibody was purchased from Sigma-Aldrich (St. Louis, MO, USA).

Cell culture

The hypothalamic N38 cell line was purchased from Cedarlane (Ontario, Canada) and cultured in Dulbecco's Modified Eagle Medium (DMEM) supplemented with 10% fetal bovine serum (FBS) and 1% penicillin–streptomycin (P/S). For butyrate treatment, cells were incubated with butyrate at 0.01 to 20 mM final concentration for 24 h period before harvested unless stated otherwise. All of cell culture experiments were performed in biological triplicate unless stated otherwise.

Animal

The Institutional Animal Care and Use Committee (IACUC) at the Avison Biomedical Research Center, Yonsei University, approved all animal protocols utilized in this research (Approval No. 2022-0056). All experiments were performed using inbred C57BL/6J mice. To generate hypothalamic primary cilia knockout mice, mice carrying the Ift88 floxed allele (Jackson Laboratory, Strain no.022409) were crossed with either AgRP-ires-cre (Jackson Laboratory, Strain no.012899) or SF-1-cre (Jackson Laboratory, Strain no.012462) mice. Whenever stated, mice were backcrossed with the Cre-dependent reporter Gt(ROSA) 26Sor (Ai9) mouse line (Jackson Laboratory, B6;129S6-Gt(ROSA) 26Sortm9(CAG-tdTomato)Hze/J, Strain no.007905) to identify cells with Cre recombinase activity using td-Tomato fluorescence. For comparisons of primary cilia length between hypothalamic AgRP/NPY and POMC neurons, heterozygous transgenic mice expressing humanized Renilla green fluorescent protein (hrGFP) under the control of the *Npy* (Jackson Laboratory, Strain no.006417) or *Pomc1* promoter (Jackson Laboratory, Strain no.006421) were used. Both male and female mice were included in metabolic phenotyping experiments, whereas male mice were used for molecular, histological, and electrophysiological analyses. Mice were housed in individual cages under the specific pathogen-free condition, with a 12:12 h light:dark cycle (light automatically on/off at 08:00–20:00) at 22 ± 1 °C and with 55% humidity. Mice were fed either a high fat diet (HFD, Research Diets, 60% calories from fat, Cat.no.D12492) or control chow diet (PicoLab® Rodent diet 20, LabDiet, 13.2% calories from fat) and provided with distilled water *ad libitum*.

For experiments with peripheral butyrate administration, 8- to 10-week-old male mice were stabilized on HFD feeding for 7 days before starting butyrate treatment. pH-matched (7.45 ± 0.03) solutions of sodium butyrate (Santa Cruz Biotechnology, Cat.no.sc-202341C) and sodium bicarbonate buffer as the control were prepared at final concentration of 100 mM and provided *ad libitum* via the drinking water

https://doi.org/10.1038/s41467-026-71745-w

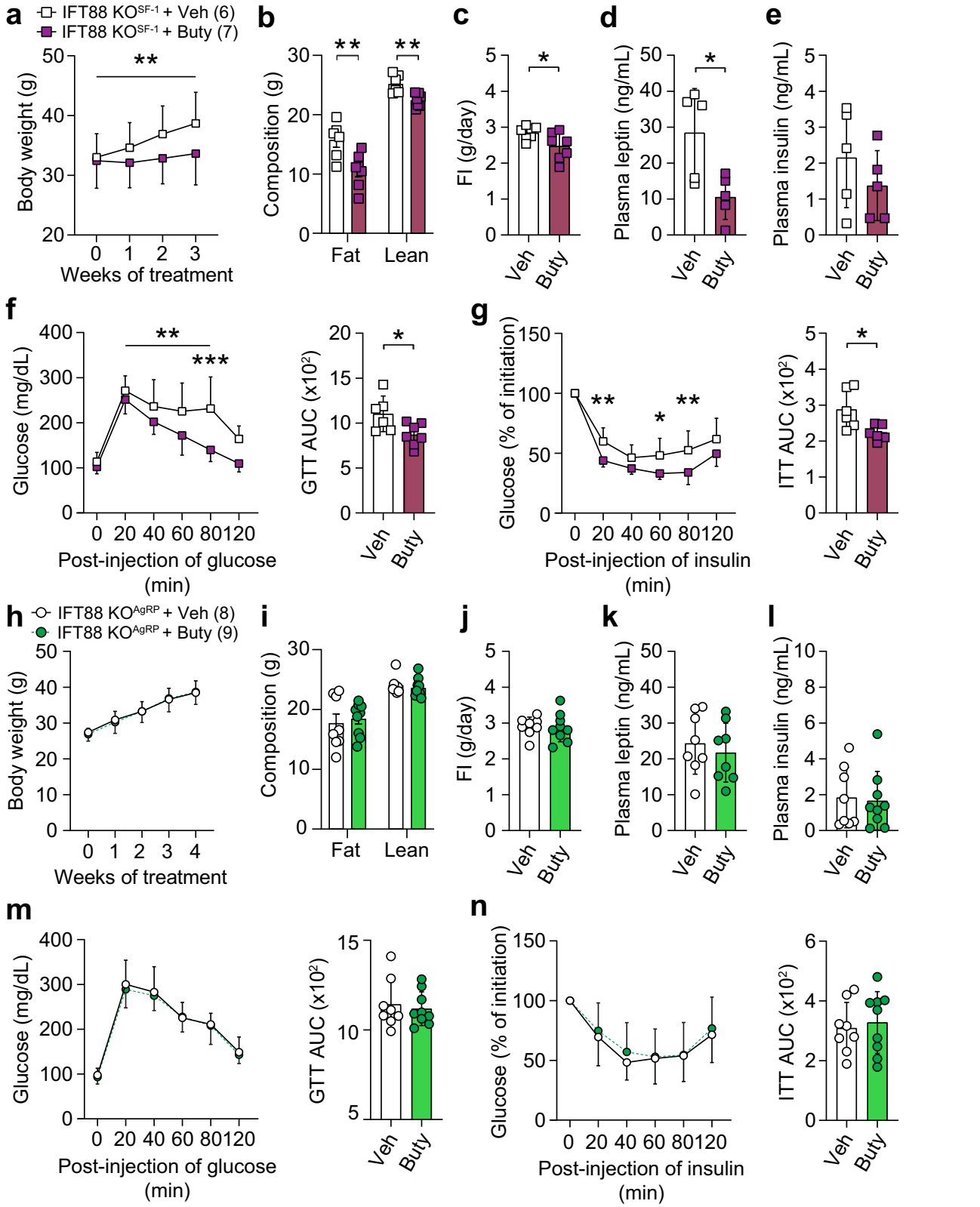

bottles. Butyrate and control solutions in drinking bottles were freshly replaced every 3 days. For experiments with i.p. butyrate administration, sodium butyrate (500 mg/kg of body weight) and sterile control saline were injected i.p. daily after measuring the body weight.

For experiments with ICV injection, mice after full recovery from ICV cannulation were stabilized on HFD feeding for 7 days before starting ICV injection treatment. 2.5 μL of 1.25 μg/μL sodium butyrate solution or control saline was daily infused via inserted ICV cannula into the third ventricle at an infusion rate of 2.5 μL/min using the microinjection syringe pump (LEGATO® 100 syringe pump, KD Scientific, MA, USA). Body weight was monitored daily before injection. At the end of experiments, mice were perfused using 10% neutral-buffered formalin solution or euthanized by decapitation. Blood plasma and tissue samples were snap frozen in dry ice and stored at

https://doi.org/10.1038/s41467-026-71745-w

Fig. 4 | Primary cilia in the hypothalamic ARC, particularly in the AgRP neurons, are required for butyrate metabolic actions. Effects of ICV butyrate treatment on body weight change (**a**) body composition (**b**) food intake (**c**) plasma leptin (**d**) and insulin levels (**e**) in IFT88 KO^{SF-1} mice under HFD feeding. Two-way repeated-measures ANOVA with Sidak's multiple comparison test (**$p = 0.0089$). Two-tailed unpaired Student's *t*-test (fat mass, **$p = 0.0092$; lean mass, **$p = 0.0036$; FI, *$p = 0.0274$; plasma leptin, *$p = 0.0197$). **f** GTT and corresponding AUC in IFT88 KO^{SF-1} mice following 3 weeks of ICV butyrate treatment (vehicle, $n = 6$; butyrate, $n = 7$). Two-way repeated measures ANOVA (**$p = 0.0070$) with Sidak's multiple comparison test for individual time points (80 min, ***$p = 0.0004$). Two-tailed unpaired Student's *t*-test (AUC, *$p = 0.0261$). **g** ITT and corresponding AUC in IFT88 KO^{SF-1} mice following 3 weeks of ICV butyrate treatment. (vehicle, $n = 6$; butyrate, $n = 7$). Two-way repeated measures ANOVA with Sidak's multiple comparison test for individual time points (20 min, **$p = 0.009$; 60 min, *$p = 0.0141$; 80 min, **$p = 0.069$). Two-tailed unpaired Student's *t*-test (AUC, *$p = 0.0202$). Effects of ICV butyrate treatment on body weight change (**h**) body composition (**i**) food intake (**j**) plasma leptin (**k**) and insulin levels (**l**) in the IFT88 KO^{AgRP} mice under HFD feeding (vehicle, $n = 8$; butyrate, $n = 9$). **m** GTT and corresponding AUC in IFT88 KO^{AgRP} mice following 3 weeks of ICV butyrate treatment (vehicle, $n = 8$; butyrate, $n = 9$). **n** ITT and corresponding AUC in IFT88 KO^{AgRP} mice following 3 weeks of ICV butyrate treatment (vehicle, $n = 8$; butyrate, $n = 9$). Numbers in parentheses indicate the number of mice used. All data are expressed as mean ± SD. The data for each figure are specified in associated Source data file.

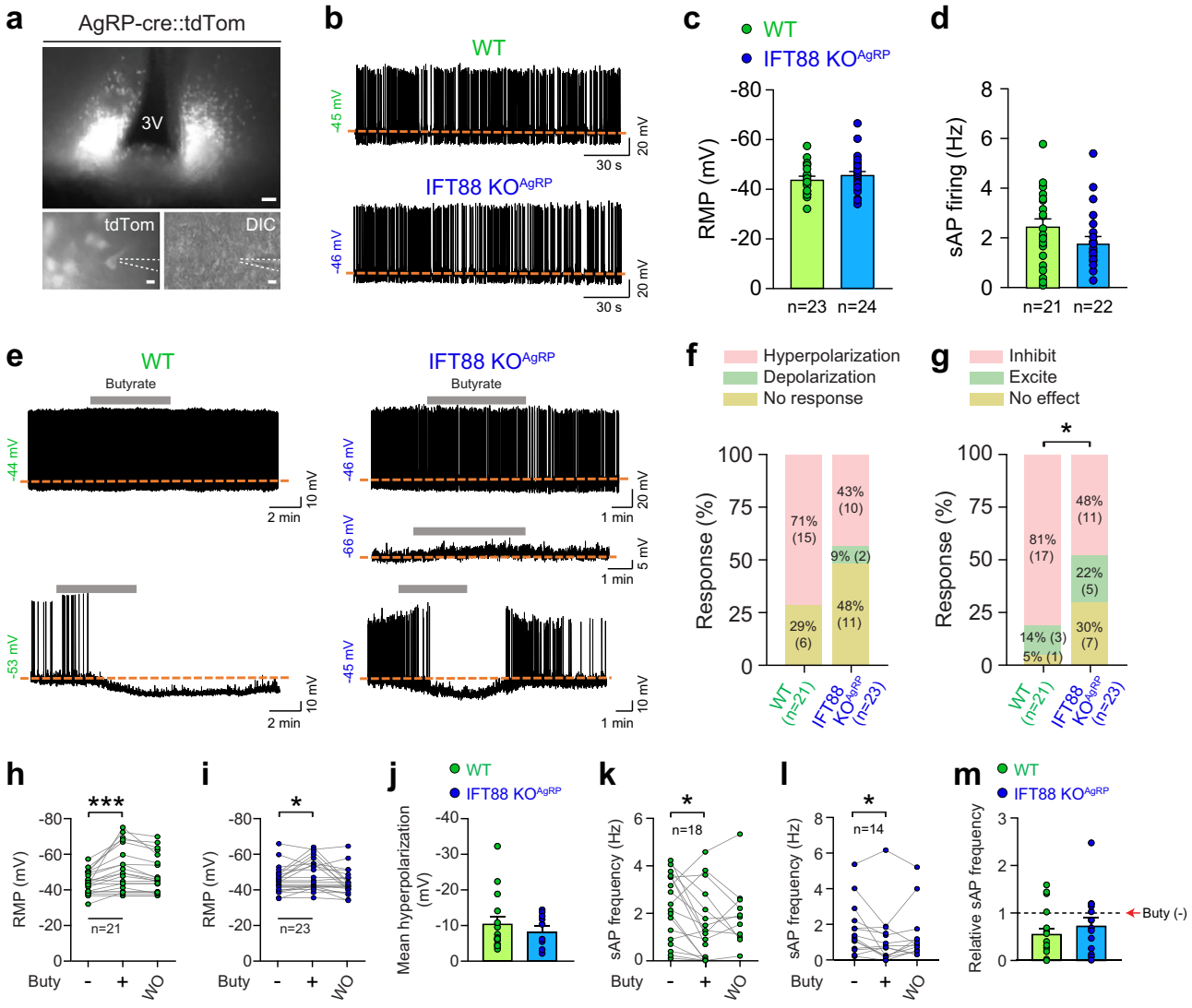

Fig. 5 | Butyrate inhibits AgRP neuronal excitability in a primary cilia-dependent manner. a Representative image showing AgRP neurons in the arcuate nucleus and a patched AgRP neuron in AgRP-Cre;tdTomato$^{F/+}$ male mice. Scale bar, 100 μm. **b** Voltage traces from wild type (WT, AgRP-Cre;tdTomato$^{F/+}$) and AgRP neuron-specific primary cilia knockout mice (IFT88 KO^{AgRP}, AgRP-Cre;IFT88$^{F/F}$;tdTomato$^{F/+}$) neurons showing resting membrane potential (RMP) and spontaneous action potential (sAP) firings. Comparison of RMP (**c**) and sAP firing frequency (**d**) between groups. **e** Voltage traces from WT and IFT88 KO^{AgRP} neurons showing heterogeneous responses to bath applied butyrate (1 mM). Horizontal bars indicate the duration of butyrate application. Percentage of WT and IFT88 KO^{AgRP} neurons exhibiting heterogeneous membrane potential change (**f**) and corresponding inhibitory or excitatory effects (**g**) in response to butyrate application. Chi-square test (*$p = 0.0449$). Note that inhibitory responses include membrane hyperpolarization and/or a reduction in sAP firing, with or without changes in RMP, while excitatory responses include membrane depolarization and/or an increase in sAP firing, with or without changes in RMP. Dot plots showing change in RMP of WT (**h**) and IFT88 KO^{AgRP} (**i**) neurons following butyrate application. Two-tailed paired Student's *t*-test (*$p = 0.0166$, ***$p = 0.0007$). WO, wash out. **j** Mean hyperpolarization induced by butyrate in WT ($n = 15$) and IFT88 KO^{AgRP} ($n = 10$) neurons. **k, l** Dot plots showing changes in sAP firings of WT (**k**) and IFT88 KO^{AgRP} (**l**) neurons under butyrate application. Two-tailed paired Student's *t*-test (*$p = 0.0147$, *$p = 0.0465$, respectively). **m** Mean relative sAP frequency in WT ($n = 18$) and IFT88 KO^{AgRP} ($n = 14$) neurons under butyrate application compared to control. Data are presented as the mean ± SEM. The data for each figure are specified in associated Source data file.

https://doi.org/10.1038/s41467-026-71745-w

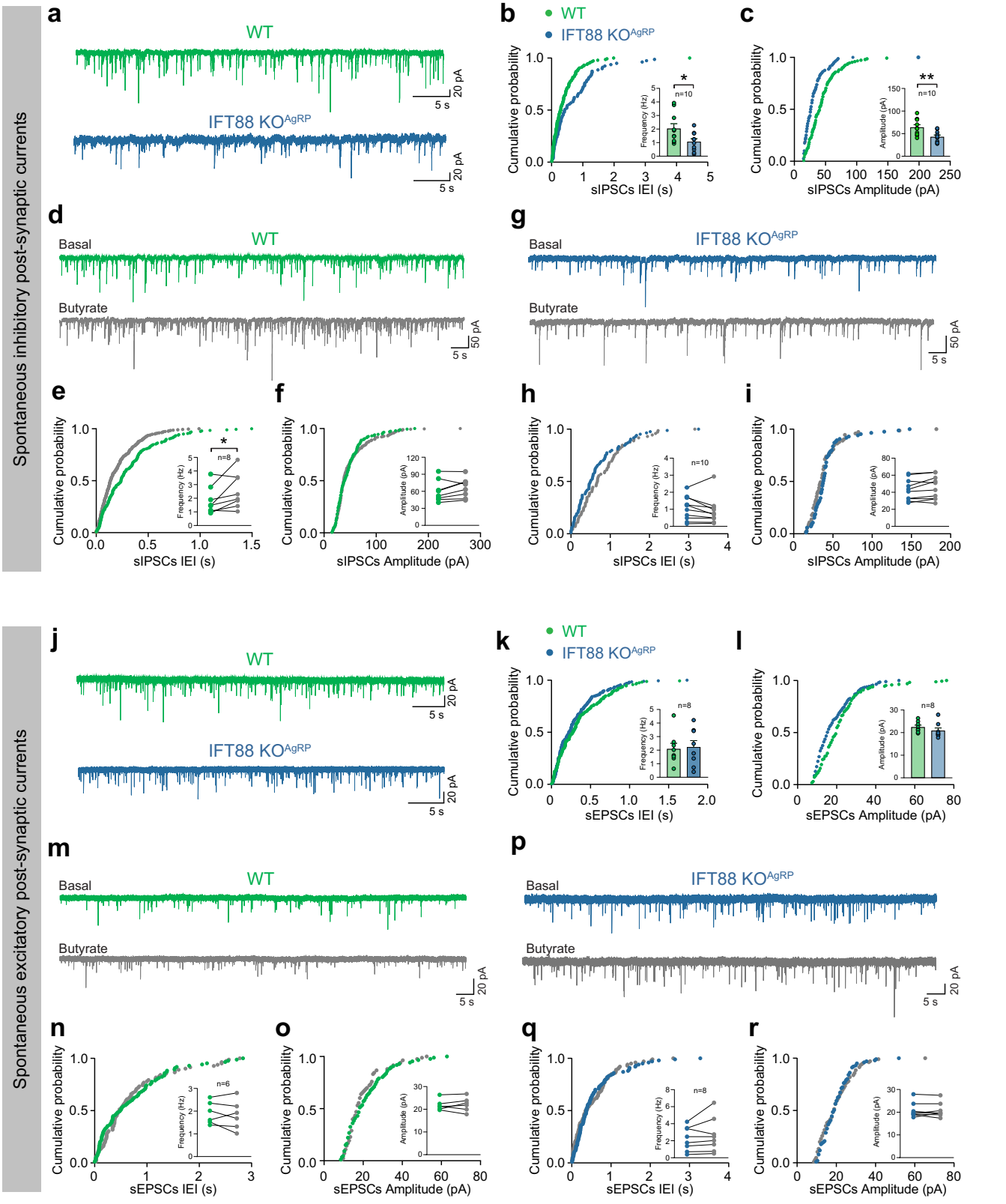

−80 °C before analyzed. Perfused organs were kept at 4 °C in the 10% neutral-buffered formalin solution.

ICV cannulation and injection procedure

Male and female mice (10–12 weeks old) were anesthetized with an i.p. injection of Zoletil and Rompun (30 and 7.5 mg/kg, respectively) and mounted on a stereotaxic frame (KOPF1900, David Kopf Instruments, CA, USA) under aseptic conditions. Guided by the Paxinos and Franklin mouse brain atlas, a 26-gauge stainless steel guide cannula was stereotaxically implanted into the third ventricle (coordinates from bregma: AP −1.8 mm, DV −5.0 mm) and secured to the skull with dental cement. Post-surgery, the animals received a single i.p. injection of ketoprofen (5 mg/kg) for analgesia and were individually housed for at least a 7-day recovery period. To verify functional cannula placement,

Fig. 6 | Butyrate enhances inhibitory synaptic transmission onto AgRP neurons via primary cilia. a Representative current traces of spontaneous inhibitory post-synaptic currents (sIPSCs) recorded from WT and IFT88 KO^{AgRP} neurons. Cumulative probability (CP) plots of inter-event intervals (IEIs) (**b**) and amplitude (**c**) for corresponding traces in (**a**). Insets show histograms of mean sIPSCs frequency and amplitude recorded from different neurons. Two-tailed unpaired Student's *t*-test (*$p = 0.0292$, **$p = 0.0070$). Representative sIPSCs traces from WT neurons under basal conditions and following butyrate application (**d**) with corresponding CP plots of IEIs (**e**) and amplitudes (**f**). Insets display dot plot for sIPSCs frequency and amplitude for all tested neurons. Two-tailed paired Student's *t*-test (*$p = 0.0480$). Representative sIPSCs traces from IFT88 KO^{AgRP} neurons under basal conditions and following butyrate application (**g**) CP plots of IEIs (**h**) and amplitudes (**i**) corresponding to the representative traces with insets showing dot plot for sIPSCs frequency and amplitude for all tested neurons. **j** Representative current traces of spontaneous excitatory post-synaptic currents (sEPSCs) recorded from WT and IFT88 KO^{AgRP} neurons. CP plots of IEIs (**k**) and amplitude (**l**) for corresponding traces in **j**. Insets show mean sEPSCs frequency and amplitude across neurons. Representative sEPSCs traces from WT neurons under basal conditions and following butyrate application (**m**) with corresponding CP plots of IEIs (**n**) and amplitudes (**o**). Insets show dot plot for sEPSCs frequency and amplitude for all tested neurons. Representative sEPSCs traces from IFT88 KO^{AgRP} neurons under basal conditions and following butyrate application (**p**) with corresponding CP plots of IEIs (**q**) and amplitudes (**r**). Insets show dot plot for sEPSCs frequency and amplitude for all tested neurons. Data are presented as the mean ± SEM. The data for each figure are specified in associated Source data file.

mice were centrally infused with angiotensin II (50 ng in 2.5 μL, rate of 2.5 μL/min). Only those exhibiting a robust dipsogenic response within 5 min were included in subsequent experiments; non-responders were excluded. Prior to the actual ICV treatments, all mice underwent three days of habituation to handling and restraint to minimize stress. Finally, the anatomical accuracy of the cannula placements was confirmed post-mortem.

Stereotaxic virus injection

Eight-week-old male mice were anesthetized via an intraperitoneal injection of a Zoletil and Rompun cocktail (30 and 7.5 mg/kg, respectively). Under aseptic conditions, the skull was exposed via a minor incision and drilled at the designated coordinates. We stereotaxically injected 500 nL of either AAV2-Cre-GFP (Addgene, Cat. No. 105545) or AAV2-GFP (Addgene, Cat. No. 105530) into the third ventricle (3 V) of the hypothalamus (AP: −1.76 mm, ML: 0 mm, DV: −5.25 mm relative to bregma). The viral vectors were delivered at a constant rate of 50 nL/min over 10 min, with the injection needle left in situ for another 5 min to prevent backflow. Post-operatively, animals recovered on a heating pad to maintain body temperature. A minimum three-week period was provided to ensure complete surgical recovery and adequate Cre expression prior to experimental interventions. Finally, accurate viral targeting in the 3 V was confirmed post-mortem using immunohistochemistry (IHC); animals with off-target injections were excluded from the final analysis.

Food intake measurement

Daily food consumption was calculated by subtracting the weight of the remaining chow from the initial amount provided every 24 h. We monitored this intake for the first 5 days following the onset of treatment and utilized the average daily consumption for our comparative analyses. To ensure data accuracy, measurements from mice exhibiting food-crumbling behavior were excluded from the final analysis.

Glucose and insulin tolerance tests

Following 3–4 weeks of butyrate administration, we conducted glucose and insulin tolerance tests (GTT and ITT). Prior to testing, mice were fasted overnight for the GTT or for 2 h for the ITT, while maintaining free access to water. Mice were i.p. injected with a solution of D-glucose (1.5 g/kg of body weight) or insulin (1.2 U/kg of body weight; HumulinR, Elli&Lilly) prepared in saline for GTTs and ITTs, respectively. Baseline (t0) and post-injection blood glucose levels were recorded at predetermined intervals by sampling tail-vein blood using a ContourTS hand-held glucometer (Bayer, Germany).

Metabolic cage study

To evaluate indirect calorimetry, HFD-fed mice receiving either butyrate or a vehicle control were placed in a 12-channel PhenoMaster Home Cage System (TSE Systems Inc.) featuring triple-beam infrared technology. The animals were single-housed and allowed to acclimatize to the metabolic chambers for 48 h under standard experimental conditions. Following this habituation, we continuously monitored various metabolic indices—including oxygen consumption (VO_2), carbon dioxide production (VCO_2), energy expenditure, locomotor activity, and ingestive behaviors (food and water intake)—over a 5-day period. Throughout the evaluation, mice had ad libitum access to chow and water.

Measurement of body composition (Dual-energy X-ray absorptiometry)

For the analysis of body composition, the fat and lean masses of the mice were quantified using a dual-energy X-ray absorptiometry (DEXA) scanner (InAlyzer™, MEDIKORS, Korea) under brief isoflurane anesthesia. Following calibration according to the manufacturer's instructions, the system's lower limit of detection was established at 0.001 g/cm^2.

Measurements of metabolic hormones

Blood samples obtained via tail-nick were collected into EDTA-treated capillary tubes (Microvette CB300, Sarstedt). Following centrifugation to isolate the plasma, the aliquots were immediately frozen and maintained at −80 °C. The circulating concentrations of insulin and leptin were subsequently quantified using commercial ELISA kits (Morinaga Institute of Biological Science, Yokohama, Japan) in strict accordance with the manufacturer's provided protocols.

Immunoblotting

Cells or tissue homogenates were washed in 1X PBS and subsequently lysed using RIPA buffer (containing 150 mM NaCl, 50 mM Tris pH 8.0, 1% Triton X-100, 0.5% sodium deoxycholate, and 0.1% SDS) enriched with phosphatase and protease inhibitor cocktails (Roche, Basel, Switzerland). Total protein concentration was determined via the Bio-Rad Protein Assay system (Bio-Rad Laboratories, CA, USA). Equivalent quantities of protein lysates were resolved by SDS-PAGE on acrylamide gels and electro transferred to nitrocellulose membranes. For blocking, the membranes were treated with 5% non-fat milk in TBST (Tris-buffered saline containing 0.1% Tween 20) before an overnight incubation at 4 °C with the respective primary antibodies under gentle agitation. After washing the membranes four times in TBST, they were exposed to species-appropriate secondary antibodies for 1 hour at room temperature on a shaker. Following an additional four washes with TBST, the protein bands were developed using an ECL substrate and captured on X-ray film or a chemiluminescence imaging platform.

Quantitative real-time PCR (qPCR)

Total RNA was isolated from cultured cells or tissue homogenates utilizing the Trizol reagent (Life Technologies, CA, USA). Following RNA quantification via a NanoDrop spectrophotometer, 0.5–1 μg of the purified RNA was converted into cDNA with the ReverTra Ace-α-™ synthesis kit (Toyobo, Osaka, Japan). The qPCR was subsequently performed on a CFX Connect Real-Time System (Bio-Rad, CA, USA). Each reaction mixture contained 1 μL of the cDNA template, target-

specific primers, and iQ SYBR Green Supermix. To ensure accurate quantification, all gene expression data were normalized to 18S ribosomal RNA (18S) as the endogenous control.

Primer sequences used in qPCR were as follows: *18S*: F, 5′-AACCCGTTGAACCCCATT-3′, R, 5′-CCATCCAATCGGTAGTAGCG-3′; *Agrp*: F, 5′-CGGCCACGAACCTCTGTAG-3′, R, 5′-CTCATCCCCTGCCTTTGC-3′; *Foxj1*: F, 5′- CCCTGACGACGTGGACTATG-3′, R, 5′- GCCGACAGAGTGATCTTGGT-3′; *Ift20:* F, 5′- AGGCAGGGCTGCATTTTGAT-3′, R, 5′- CAAGCTCAATTAGACCACCAACA-3′; *Ift27*: F, 5′- GGGACCCATTTCCAGAAGAA-3′, R, 5′- CCGGCTGAGTCAAAAATGAA-3′; *Ift54*: F, 5′- TGTGTAAGAGTGCGCTTCCC-3′, R, 5′- GCATGCTGCCTGTTCTCACT-3′; *Ift88*: F, 5′- GCAGTGACAGTGGCCAGAAC-3′, R, 5′- AAGGTTCATCTGTCCCAGGC-3′; *Kif3a:* F, 5′- AGCTGCGATAATGTGAAGGTG-3′, R, 5′- GTTCCCCTCATTTCATCCACG-3′; *Kif3b*: F, 5′- GGACTGTGTGTGGAGCCTTG-3′, R, 5′- CTGACAGAGGCAGGCACCTA-3′; *Npy*: F, 5′-CTACTCCGCTCTGCGACACT-3′, R, 5′-AGTGTCTCAGGGCTGGATCTC-3′; *Pomc*: F, 5′-CAGGTCCTGGAGTCCGAC-3′, R, 5′-CATGAAGCCACCGTAACG-3′; *Rfx1:* F, 5′- GGCAGCCAGAAGCAGTATGT-3′, R, 5′- GCACCTTCCGATACGGTGA-3′; *Rfx2:* F, 5′- TGTGAGCCGATCCTACAGTG-3′, R, 5′- CCGCAGCACATCTGGGATAAG-3′; *Rfx3:* F, 5′- AGCTCGGGAGGAACCTATTTG-3′, R, 5′- GACAGACCGTCAGACTTTTGC-3′; and *Rfx4:* F, 5′- GACAGCTTAACTCAGGTGATCC-3′, R, 5′- GTTTTCCGGGAGATCGTGGAG-3′.

Immunofluorescence (IF) staining and quantification of cilia length

Cells grown on coverslips were fixed with 4% paraformaldehyde (PFA) for 10 minutes at room temperature, followed by an overnight incubation at 4 °C with an anti-acetylated-α-tubulin antibody under gentle agitation. For brain tissue analysis, mice underwent transcardial perfusion with 10% neutral-buffered formalin (Sigma-Aldrich, MO, USA). Extracted whole brains were cryoprotected overnight in a 20% sucrose/PBS solution and subsequently sliced into 25-μm sections utilizing a Leica CM1850 cryostat (Wetzlar, Germany). Fixed cells or brain sections were blocked in 3% goat serum prepared in 1X PBS with 0.25% Triton® X-100 (0.25% PBST) for 1 h and incubated with the acetylated-α-tubulin antibody (for staining primary cilia in cells) or the adenylyl cyclase III antibody (for staining primary cilia in brain sections) prepared in PBST for 24 h at 4 °C on a shaker. After washing 4 times with 1X PBS, cells or brain sections were incubated with the Alexa Fluor 488 secondary antibody (Invitrogen, CA, USA) prepared in 0.1% PBST. After washing 4 times (10 min for each) with 1X PBS, cover glasses of stained cells and brain sections were mounted using the Fluoroshield Mounting Medium with DAPI (Abcam, Cat.-no.ab188804) and visualized with the Zeiss LSM700 Confocal Laser Scanning Microscope. Captured images generated from the ZEN 3.0 SR software of the microscope system were subjected to the ImageJ CiliaQ Plugins software tool (https://github.com/hansenjn/CiliaQ) for an automated quantification of ciliary length[57] or analyzed by an independent researcher without prior knowledge of experiment identity.

Histological analysis

White adipose tissues collected in 10% neutral-buffered formalin solution were paraffin embedded, sectioned, and stained with hematoxylin and eosin (H&E) following a standard protocol. Stained samples were visualized and captured by the Leica ICC50E microscope system (Leica Microsystems, Wetzlar, Germany). Captured images were subjected to the ImageJ Adiposoft Plugin software tool (https://imagej.net/plugins/adiposoft) for an automated quantification of adipocyte and lipid droplet size[58].

Brain slice preparation and electrophysiology

Five to seven-weeks-old male WT (AgRP-cre;tdTomato$^{F/+}$) or IFT88 KO^{AgRP} (AgRP-cre;IFT88$^{F/F}$;tdTomato$^{F/+}$) mice carrying a Cre-dependent tdTomato reporter allele were used for electrophysiological experiments. For slice preparation, mice were decapitated, and their dissected brains were quickly immersed in ice-cold, oxygenated cutting solution containing (in mM): 208 Sucrose, 2.5 KCl, 0.5 $CaCl_2$, 6 $MgCl_2$, 11 D-glucose, 1.4 NaH_2PO_4, 25 $NaHCO_3$, and 0.5 sodium ascorbate. Coronal hypothalamic slices (300 μm thick) were prepared using a vibratome (7000SMZ-2, Campden Instruments, Loughborough, England). The slices were then incubated at 30 °C for 1 h in oxygenated artificial cerebrospinal fluid (ACSF) with composition (in mM): 126 NaCl, 2.5 KCl, 2.4 $CaCl_2$, 1.2 $MgCl_2$, 11 D-glucose, 1.4 NaH_2PO_4, 25 $NaHCO_3$, and 0.5 sodium ascorbate (osmolarity 310–320 mOsm, pH 7.3–7.4, bubbled with 95% O_2/5% CO_2).

For recordings, slices were transferred to a recording chamber perfused with oxygenated ACSF at a flow rate of approximately 2 mL/min using a gravity-driven perfusion system. AgRP-expressing neurons in the arcuate nucleus (ARC) were identified via brief epifluorescence exposure on a Nikon FN1 upright microscope (Nikon Instruments Inc., Melville, NY, USA) equipped with a 10× water-immersion objective and differential interference contrast optics. Whole-cell signals were amplified using a Multiclamp 700B amplifier (Molecular Devices), filtered at 2 kHz, and digitized at 10 kHz using a Digidata 1440 A interface (Molecular Devices). Recording pipettes, fabricated from borosilicate glass using a Flaming-Brown puller (P-1000, Sutter Instruments), had a tip resistance of 3–5 MΩ. The standard pipette solution contained (in mM): 130 K-gluconate, 10 KCl, 1 $CaCl_2$, 1 $MgCl_2$, 10 HEPES, 4 MgATP, and 10 EGTA, with the pH adjusted to 7.3 using KOH, for current clamp data and spontaneous excitatory post-synaptic currents (sEPSCs) under voltage clamp mode at −70 mV. sEPSCs were recorded in the presence of 100 μM picrotoxin (PTX) in ACSF. For recording spontaneous inhibitory post-synaptic currents (sIPSCs), ACSF containing 10 μM 6-cyano-7-nitroquinoxaline-2,3-dione (CNQX) and 50 μM D-2-amino-5-phosphonopentanoic acid (DL-AP5) was used, along with a high-Cl^- intracellular pipette solution (130 mM KCl replacing K-gluconate). Under the high [Cl^-], the reversal potential for Cl^- was 0 mV, resulting in inward $GABA_A$ -mediated currents at −70 mV. All recordings were performed at room temperature using pCLAMP 10.7 software (Molecular Devices). Resting membrane potential (RMP) and action potential (AP) firing properties were assessed after 5 min of whole-cell configuration. Series resistance (Rs) was monitored at the beginning and end of each experiment, and data were discarded if neurons exhibited Rs greater than 20 MΩ or if it changed by more than 20% during the recording. A neuron was classified as depolarized or hyperpolarized if its RMP shifted by at least 2 mV. Membrane potentials were not corrected for liquid junction potential (−8 mV). AP firing frequency, as well as synaptic current frequency and amplitude, were analyzed using Mini Analysis software (ver. 6.0.7; Synaptosoft Inc., Decatur, GA, USA).

Statistics

Statistical significance was determined using Student's *t*-test, chi-square test, and two-way ANOVA, as appropriate, using GraphPad Prism 8.0 software (GraphPad Software, Inc., CA, USA). Detailed statistical test(s) used, and corresponding *p*-value are described in figure legends. For all analyses, $p < 0.05$ was considered statistically significant.

Reporting summary

Further information on research design is available in the Nature Portfolio Reporting Summary linked to this article.

Data availability

All data generated in this study are included in the Source data file. Additional information or materials related to this study are available from the corresponding author. Source data are provided with this paper.

References

1. Dalile, B., Van Oudenhove, L., Vervliet, B. & Verbeke, K. The role of short-chain fatty acids in microbiota-gut-brain communication. *Nat. Rev. Gastroenterol. Hepatol.* **16**, 461–478 (2019).
2. van der Hee, B. & Wells, J. M. Microbial regulation of host physiology by short-chain fatty acids. *Trends Microbiol.* **29**, 700–712 (2021).
3. Müller, M. et al. Circulating but not faecal short-chain fatty acids are related to insulin sensitivity, lipolysis and GLP-1 concentrations in humans. *Sci. Rep.* **9**, 12515 (2019).
4. Li, Z. et al. Butyrate reduces appetite and activates brown adipose tissue via the gut-brain neural circuit. *Gut* **67**, 1269–1279 (2018).
5. Lucas, S. et al. Short-chain fatty acids regulate systemic bone mass and protect from pathological bone loss. *Nat. Commun.* **9**, 55 (2018).
6. Donohoe, D. R. et al. The microbiome and butyrate regulate energy metabolism and autophagy in the mammalian colon. *Cell Metab.* **13**, 517–526 (2011).
7. Li, B. et al. Microbiota depletion impairs thermogenesis of brown adipose tissue and browning of white adipose tissue. *Cell Rep.* **26**, 2720–2737. e2725 (2019).
8. Arnoldussen, I. A. et al. Butyrate restores HFD-induced adaptations in brain function and metabolism in mid-adult obese mice. *Int. J. Obes.* **41**, 935–944 (2017).
9. Gao, Z. et al. Butyrate improves insulin sensitivity and increases energy expenditure in mice. *Diabetes* **58**, 1509–1517 (2009).
10. De Vadder, F. et al. Microbiota-generated metabolites promote metabolic benefits via gut-brain neural circuits. *Cell* **156**, 84–96 (2014).
11. Ashwini, K. et al. Molecular basis of the therapeutic effect of butyrate in glioblastoma revealed by in vitro and in silico approach. *Biochem. Biophys. Res. Commun.* **777**, 152216 (2025).
12. Oldendorf, W. H. Carrier-mediated blood-brain barrier transport of short-chain monocarboxylic organic acids. *Am. J. Physiol.* **224**, 1450–1453 (1973).
13. Kekuda, R., Manoharan, P., Baseler, W. & Sundaram, U. Monocarboxylate 4 mediated butyrate transport in a rat intestinal epithelial cell line. *Dig. Dis. Sci.* **58**, 660–667 (2013).
14. Frost, G. et al. The short-chain fatty acid acetate reduces appetite via a central homeostatic mechanism. *Nat. Commun.* **5**, 3611 (2014).
15. Koh, A., De Vadder, F., Kovatcheva-Datchary, P. & Bäckhed, F. From dietary fiber to host physiology: short-chain fatty acids as key bacterial metabolites. *Cell* **165**, 1332–1345 (2016).
16. Krautkramer, K. A. et al. Diet-microbiota interactions mediate global epigenetic programming in multiple host tissues. *Mol. Cell* **64**, 982–992 (2016).
17. Zhou, Z. et al. Sodium butyrate attenuated neuronal apoptosis via GPR41/Gβγ/PI3K/Akt pathway after MCAO in rats. *J. Cereb. Blood Flow. Metab.* **41**, 267–281 (2021).
18. Volmar, C.-H. & Wahlestedt, C. Histone deacetylases (HDACs) and brain function. *Neuroepigenetics* **1**, 20–27 (2015).
19. Stilling, R. M. et al. The neuropharmacology of butyrate: the bread and butter of the microbiota-gut-brain axis?. *Neurochem Int.* **99**, 110–132 (2016).
20. Lam, H. C. et al. Histone deacetylase 6–mediated selective autophagy regulates COPD-associated cilia dysfunction. *J. Clin. Investig.* **123**, 5212–5230 (2013).
21. Kobayashi, T. et al. HDAC 2 promotes loss of primary cilia in pancreatic ductal adenocarcinoma. *EMBO Rep.* **18**, 334–343 (2017).
22. Smith, Q. et al. Differential HDAC6 activity modulates ciliogenesis and subsequent mechanosensing of endothelial cells derived from pluripotent stem cells. *Cell Rep.* **24**, 895–908. e896 (2018).
23. Peixoto, E. et al. HDAC6-dependent ciliophagy is involved in ciliary loss and cholangiocarcinoma growth in human cells and murine models. *Am. J. Physiol. Gastrointest. Liver Physiol.* **318**, G1022–G1033 (2020).
24. Gradilone, S. A. et al. HDAC6 inhibition restores ciliary expression and decreases tumor growth. *Cancer Res.* **73**, 2259–2270 (2013).
25. Xiang, W. et al. HDAC6 inhibition suppresses chondrosarcoma by restoring the expression of primary cilia. *Oncol. Rep.* **38**, 229–236 (2017).
26. Nishimura, Y., Kasahara, K., Shiromizu, T., Watanabe, M. & Inagaki, M. Primary cilia as signaling hubs in health and disease. *Adv. Sci.* **6**, 1801138 (2019).
27. Youn, Y. H. & Han, Y.-G. Primary cilia in brain development and diseases. *Am. J. Pathol.* **188**, 11–22 (2018).
28. Berbari, N. F., Lewis, J. S., Bishop, G. A., Askwith, C. C. & Mykytyn, K. Bardet–Biedl syndrome proteins are required for the localization of G protein-coupled receptors to primary cilia. *Proc. Natl. Acad. Sci. USA* **105**, 4242–4246 (2008).
29. Omori, Y. et al. Identification of G protein-coupled receptors (GPCRs) in primary cilia and their possible involvement in body weight control. *PLoS ONE* **10**, e0128422 (2015).
30. Loktev, A. V. & Jackson, P. K. Neuropeptide Y family receptors traffic via the Bardet-Biedl syndrome pathway to signal in neuronal primary cilia. *Cell Rep.* **5**, 1316–1329 (2013).
31. Guo, D.-F. et al. The BBSome controls energy homeostasis by mediating the transport of the leptin receptor to the plasma membrane. *PLoS Genet.* **12**, e1005890 (2016).
32. Siljee, J. E. et al. Subcellular localization of MC4R with ADCY3 at neuronal primary cilia underlies a common pathway for genetic predisposition to obesity. *Nat. Genet.* **50**, 180–185 (2018).
33. Oh, E. C., Vasanth, S. & Katsanis, N. Metabolic regulation and energy homeostasis through the primary Cilium. *Cell Metab.* **21**, 21–31 (2015).
34. Davenport, J. R. et al. Disruption of intraflagellar transport in adult mice leads to obesity and slow-onset cystic kidney disease. *Curr. Biol.* **17**, 1586–1594 (2007).
35. Guo, D.-F. et al. The BBSome in POMC and AgRP neurons is necessary for body weight regulation and sorting of metabolic receptors. *Diabetes* **68**, 1591–1603 (2019).
36. Han, Y. M. et al. Leptin-promoted cilia assembly is critical for normal energy balance. *J. Clin. Investig.* **124**, 2193–2197 (2014).
37. Lee, C. H. et al. Primary cilia mediate early life programming of adiposity through lysosomal regulation in the developing mouse hypothalamus. *Nat. Commun.* **11**, 5772 (2020).
38. Sun, J. S. et al. Ventromedial hypothalamic primary cilia control energy and skeletal homeostasis. *J. Clin. Investig.* **131**, e138107 (2021).
39. Yang, D. J., Hong, J. & Kim, K. W. Hypothalamic primary cilium: a hub for metabolic homeostasis. *Exp. Mol. Med.* **53**, 1109–1115 (2021).
40. Engelhard, H. H., Duncan, H. A., Kim, S., Criswell, P. S. & Van Eldik, L. Therapeutic effects of sodium butyrate on glioma cells in vitro and in the rat C6 glioma model. *Neurosurgery* **48**, 616–625 (2001).
41. Simon-O'Brien, E. et al. The histone deacetylase inhibitor sodium butyrate decreases excessive ethanol intake in dependent animals. *Addict. Biol.* **20**, 676–689 (2015).
42. Yang, D. J. et al. Primary cilia regulate adaptive responses to fasting. *Metabolism* **135**, 155273 (2022).
43. Choksi, S. P., Lauter, G., Swoboda, P. & Roy, S. Switching on cilia: transcriptional networks regulating ciliogenesis. *Development* **141**, 1427–1441 (2014).
44. Thomas, J. et al. Transcriptional control of genes involved in ciliogenesis: a first step in making cilia. *Biol. Cell* **102**, 499–513 (2010).
45. Dienel, G. A., Liu, K. & Cruz, N. F. Local uptake of 14C-labeled acetate and butyrate in rat brain in vivo during spreading cortical depression. *J. Neurosci. Res.* **66**, 812–820 (2001).
46. Vien, T. N., Ta, M. C., Kimura, L. F., Onay, T. & DeCaen, P. G. Primary cilia TRP channel regulates hippocampal excitability. *Proc. Natl. Acad. Sci. USA* **120**, e2219686120 (2023).

47. Bourassa, M. W., Alim, I., Bultman, S. J. & Ratan, R. R. Butyrate, neuroepigenetics and the gut microbiome: can a high fiber diet improve brain health?. *Neurosci. Lett.* **625**, 56–63 (2016).
48. Allison, M. B. & Myers, M. G. Jr Connecting leptin signaling to biological function. *J. Endocrinol.* **223**, T25 (2014).
49. Buettner, C. et al. Critical role of STAT3 in leptin's metabolic actions. *Cell Metab.* **4**, 49–60 (2006).
50. Hong, J. et al. Butyrate alleviates high fat diet-induced obesity through activation of adiponectin-mediated pathway and stimulation of mitochondrial function in the skeletal muscle of mice. *Oncotarget* **7**, 56071 (2016).
51. Lin, H. V. et al. Butyrate and propionate protect against diet-induced obesity and regulate gut hormones via free fatty acid receptor 3-independent mechanisms. *PloS ONE* **7**, e35240 (2012).
52. Sun, B. et al. Sodium butyrate protects against high-fat diet-induced oxidative stress in rat liver by promoting expression of nuclear factor E2-related factor 2. *Br. J. Nutr.* **122**, 400–410 (2019).
53. Lang, P., Hasselwander, S., Li, H. & Xia, N. Effects of different diets used in diet-induced obesity models on insulin resistance and vascular dysfunction in C57BL/6 mice. *Sci. Rep.* **9**, 19556 (2019).
54. Egorin, M. J., Yuan, Z.-M., Sentz, D. L., Plaisance, K. & Eiseman, J. L. Plasma pharmacokinetics of butyrate after intravenous administration of sodium butyrate or oral administration of tributyrin or sodium butyrate to mice and rats. *Cancer Chemother. Pharm.* **43**, 445–453 (1999).
55. Nishitsuji, K. et al. Analysis of the gut microbiome and plasma short-chain fatty acid profiles in a spontaneous mouse model of metabolic syndrome. *Sci. Rep.* **7**, 15876 (2017).
56. Diepenbroek, C. et al. Validation and characterization of a novel method for selective vagal deafferentation of the gut. *Am. J. Physiol. Gastrointest. Liver Physiol.* **313**, G342–G352 (2017).
57. Hansen, J. N., Rassmann, S., Stüven, B., Jurisch-Yaksi, N. & Wachten, D. CiliaQ: a simple, open-source software for automated quantification of ciliary morphology and fluorescence in 2D, 3D, and 4D images. *Eur. Phys. J. E Soft Matter* **44**, 1–26 (2021).
58. Galarraga, M. et al. Adiposoft: automated software for the analysis of white adipose tissue cellularity in histological sections. *J. Lipid Res.* **53**, 2791–2796 (2012).

Acknowledgements

This research was funded by the National Research Foundation of Korea (NRF) grants: RS-2022-NR072406 to D.J.Y.; RS-2024-00338986 to D.M.S.; and RS-2022-KH129544, RS-2024-00346807, RS-2024-00399237, and RS-2025-18362970 to K.W.K.

Author contributions

S.R. performed electrophysiology experiments, analyzed data, and wrote and edited the manuscript. D.J.Y. and S.H.L. prepared animals, performed experiments, analyzed data, and arranged the figures. K.V.D. performed experiments, analyzed data, wrote the manuscript. A.L. conducted in vivo experiments involving oral butyrate treatment. Y.H.C. and D.M.S. conceptualized the project and contributed to manuscript review and editing. K.W.K. conceived the research idea, managed the project, wrote the manuscript, and edited the final version.

Competing interests

The authors declare no competing interests.

Additional information

Supplementary information The online version contains supplementary material available at https://doi.org/10.1038/s41467-026-71745-w.

Correspondence and requests for materials should be addressed to Ki Woo Kim.

Peer review information *Nature Communications* thanks Luis Varela and the other anonymous reviewer(s) for their contribution to the peer review of this work. A peer review file is available.